Anisotropic Continuous-scale Morphology

Abstract. We describe a new approach to incorporate adaptivity into the partial differential equations (PDEs) of morphological dilation and erosion. By multiplication of the image gradient with a space-variant matrix, the speed of the evolution is locally adapted to the data. This is used to create anisotropic morphological evolutions that enhance coherent, flow-like image structures. We show that our adaptive method can be implemented by means of a simple modification of the classical Rouy-Tourin finite difference scheme. Numerical experiments confirm that the proposed dilations and erosions are capable of real anisotropic behaviour that can be used for closing interrupted lines.

1 Introduction

Mathematical morphology is concerned with image analysis of shapes. It is one of the oldest and most successful areas of digital image processing; see e.g. the textbooks [6, 9, 17–19] for an overview. Its fundamental operations are called dilation and erosion. They form the basis of many other morphological processes such as openings, closings, top hats and morphological derivative operators.

Dilation and erosion are frequently implemented by algebraic set operations, see e.g. [19] for a detailed overview. However, for convex structuring elements tB with a mask B and a scaling parameter $t>0$, there is also an alternative formulation in terms of partial differential equations (PDEs) [1, 2, 5, 16, 20]: Consider some initial greyscale image $f(x, y)$, a disk

$$B := \left\{ \mathbf{z} \in \mathbb{R}^2,\ |\mathbf{z}| \leq 1 \right\}, \tag{1}$$

and the evolution equations

$$\partial_t u = \pm |\nabla u|, \tag{2}$$

where $\nabla = (\partial_x, \partial_y)^\top$ denotes the spatial nabla operator. Moreover, assume that at "time" $t = 0$, the evolution is initialised with $f(x, y)$:

$$u(x, y, 0) = f(x, y). \tag{3}$$

Then the solution $u(x, y, t)$ at time $t > 0$ gives the dilation (for the plus sign) or erosion (for the minus sign) with a disk of radius t.

PDEs of this type using a continuous scaling parameter t for the structuring element create a *continuous-scale morphology*. They offer advantages when non-digitally scalable structuring elements such as disks or ellipses are desirable, or subpixel accuracy is required.

So far continuous-scale morphology is mainly used in a non-adaptive fashion where all locations are treated equally. In other image analysis areas such as diffusion filtering, however, interesting results have been obtained by replacing homogeneous processes by space-variant [13] or even direction-variant *(anisotropic)* ones [21]. The latter ones can be used for processing anisotropic image features such as coherent, flow-like structures. Some first attempts have been made to extend such anisotropic ideas into morphological shock filters that switch locally between dilation or erosion processes [23]. However, even in this case the underying morphological processes use a nonadaptive structuring element, and adaptivity only results from the fact that the shock fronts limit dilation and erosion. Similar shape restrictions are used for the recently introduced *morphological amoebae* [10] that are described in a set-theoretic framework.

The goal of the present paper is to introduce a space-variant anisotropic behaviour directly into the PDEs of dilation and erosion. In this way one benefits from the advantages of continous-scale morphology, and creates real anisotropic behaviour without the need to impose explicit or implicit shape restrictions.

We study a generalisation of (2) enabling the implementation of dilation or erosion processes adapted to the local structure of a given image. To this end, we consider *adaptive norms* by multiplying ∇u with a suitable matrix $\mathbf{D}$, yielding the new PDEs

$$\partial_t u = \pm |\mathbf{D}\nabla u| \,. \tag{4}$$

The purpose of (4) is to obtain a morphological approach to *coherence-enhancement*. This is of importance in order to reconstruct interrupted anisotropic image structures. We introduce a corresponding model of the matrix $\mathbf{D}$ using information from local structure tensors [4, 8, 15].

Our paper is organised as follows. After a detailed discussion of the interpretation of (4) and the modeling of $\mathbf{D}$ in Section 2, we present a numerical approximation of (4) as well as some numerical experiments in Section 3 and 4, respectively. The paper is finished by concluding remarks in Section 5.

2 Interpretation and Modelling

As can easily be shown, the introduction of a matrix $\mathbf{D}$ in (4) is equivalent with the multiplication of $|\nabla u|$ with a function $\kappa \geq 0$, where κ is defined by the deformation of the unit circle by $\mathbf{D}$ in direction of the normalised gradient:

$$|\mathbf{D}\nabla u| \;=\; \left|\mathbf{D}\frac{\nabla u}{|\nabla u|}\,|\nabla u|\right| \;=\; \underbrace{\frac{|\mathbf{D}\nabla u|}{|\nabla u|}}_{=:\,\kappa}\,|\nabla u| \;. \tag{5}$$

So, in effect, we have

$$\partial_t u\,(x,y,t) \;=\; \pm\,\kappa\,(x,y,t)\,|\mathbf{D}\nabla u\,(x,y,t)| \tag{6}$$

with a scaling function κ. However, the formulation using the matrix $\mathbf{D}$ is appropriate for our purpose since we will incorporate directional information into our model by the use of structure tensors.

Important modeling ingredients are the following. As the norm of a matrix $\mathbf{D}$ is defined by considering the deformation of the unit circle, we obtain

$$0 \leq \kappa = \frac{|\mathbf{D}\nabla u|}{|\nabla u|} \leq \max_{\mathbf{v}\neq\mathbf{0}} \frac{|\mathbf{D}\mathbf{v}|}{|\mathbf{v}|} = \|\mathbf{D}\|\,. \tag{7}$$

Now, instead of stretching the unit circle in a desired direction, we consider *normalised matrices* $\mathbf{D}$, so that we (i) keep a maximal signal speed by $\|\mathbf{D}\| = \|\mathbf{I}\| = 1$, and (ii) attenuate the flow given by $|\nabla u|$ at non-coherent image structures.

This desired behaviour is modeled by use of the *structure tensor* $\mathcal{S}$, see [4, 8, 15]. It is given by the 2×2-matrix

$$\mathcal{S} := \mathcal{K}_\rho * \left(\nabla u_\sigma \nabla u_\sigma^T\right)\,, \tag{8}$$

where ∇u_σ is the gradient of the image u pre-smoothed by a Gaussian kernel with variance σ, and where $\mathcal{K}_\rho *$ describes an analogous, element-wise convolution with a Gaussian. In this context, ρ is the so-called *integration scale*.

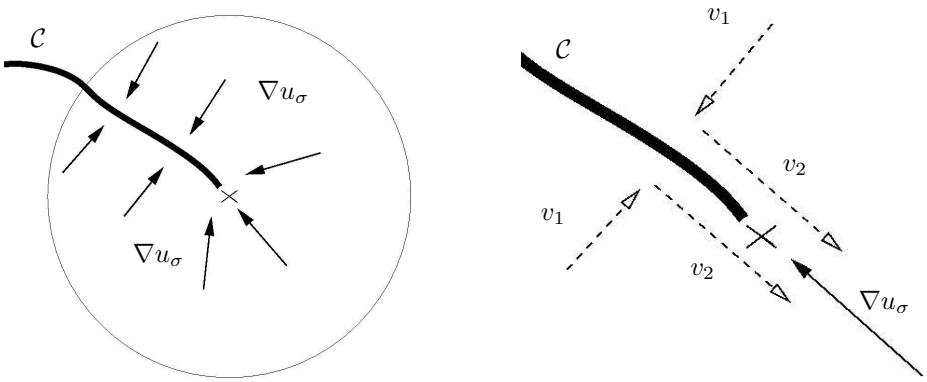

Fig. 1. (a) Left: Coherent structure $\mathcal{C}$ (thick line) together with image gradients (black arrows) and integration scale (circle) around marked point. **(b) Right:** Zoom into region around marked point, with representants of v_1, v_2 (dotted arrows) and image gradient ahead of $\mathcal{C}$ (black arrow).

Choosing, without a loss of generality, $\lambda_1 \geq \lambda_2$ for the two eigenvalues of $\mathcal{S}$, important information about the structure of the image u is then inferred from the two eigenvectors v_1, v_2: v_1 describes the orientation of highest contrast variation within the window given by the integration scale ρ, and $v_2 \perp v_1$.

Let us stress that the purpose of the structure tensor is robust estimation of directional information in an image. The pre-smoothing of u is done to attenuate sensitivity to noise. The decisive step in the construction of the structure

tensor is the subsequent averaging over a neighborhood conveniently achieved by componentwise convolution with a Gaussian of width ρ, the *integration scale* as displayed in (8). This especially has the effect that the eigenvector for the larger eigenvalue of $\mathcal{S}$ is a reliable estimate of the direction of features in the neighborhood, more robust than the direct average of the gradients itself.

What is the role of the integration scale? Let us stress explicitly, that v_1 and v_2 are supposed to incorporate orientation information on a *larger scale*, determined by ρ in (8), in comparison to the more *local* gradient information given by ∇u_σ. The parameter σ determining the pre-smoothing is usually chosen relatively small (≤ 1), while typical integration scales we have employed for numerical testing are $\rho \geq 3$. The idea followed in this paper is to compare pointwise an *average orientation* given by v_1, v_2 (where we make use, especially, of v_2), with *local orientations* given by ∇u_σ, compare Figure 1.

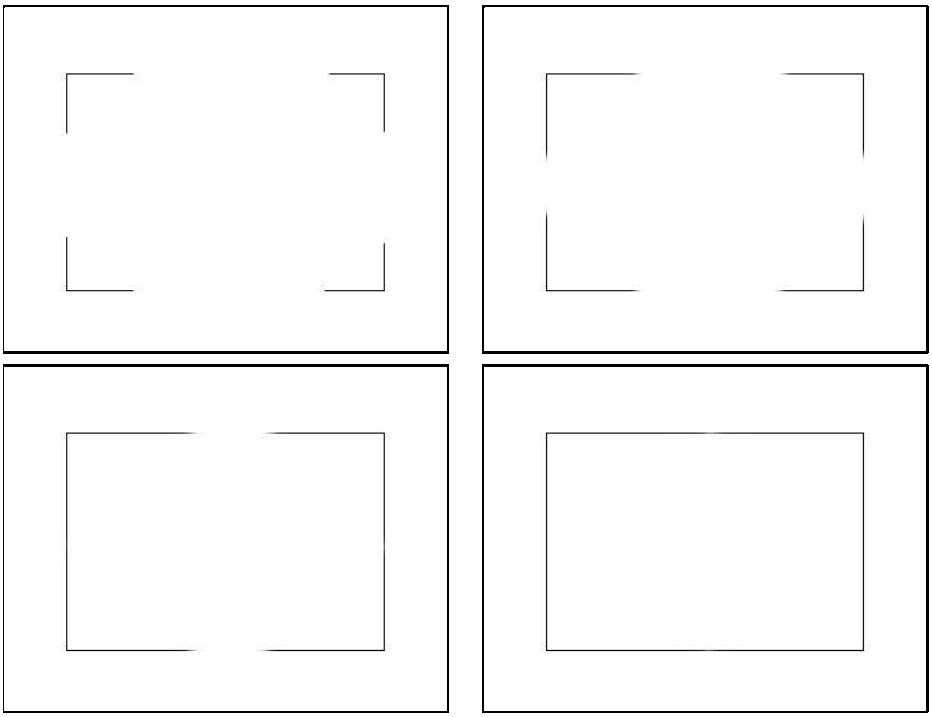

Fig. 2. (a) Top left: Initial image, 385×300 pixels. **(b) Top right:** Eroded image after 40 time steps. **(c) Bottom left:** After 100 time steps. **(d) Bottom left:** After 170 time steps.

Is the selection of the integration scale related to the size of gaps in coherent structures? The answer is *no*. The integration scale is only of importance in its role computing (8). This is confirmed by a simple illusory contour type experiment in Figure 2: while the integration scale is given by $\rho = 4$, i.e., practically, it is limited by 12 pixels after truncating the Gaussian

convolution kernel, the gaps that are going to be closed have widths of about $100 - 200$ pixels. The figure displays the temporal evolution of an anisotropic erosion process.

How do we implement orientation information in our model? As illustrated by Figure 1 (b), directly at the end of a coherent structure the vectors v_2 and ∇u_σ have approximately the same *orientation*, but they do not necessarily point in the same direction. In this situation, the function η,

$$\eta\left(v_2, \nabla u_\sigma\right) := \left|\cos \angle\left(v_2, \nabla u_\sigma\right)\right| = \left| \frac{\langle v_2, \nabla u_\sigma \rangle}{|v_2| \cdot |\nabla u_\sigma|} \right| , \tag{9}$$

where $\langle \cdot, \cdot \rangle$ denotes the inner product of vectors, is close to 1. Note, that we suppressed for the sake of brevity the dependence of η on space and time variables. If ∇u_σ is evaluated at points not too close to the end of $\mathcal{C}$, then $0 \leq \eta \ll 1$ will hold. In order to enforce a strong damping of the function η in this case, we exponentiate η by a nonnegative integer μ. The influence of μ on the quality of numerical results is shown in Figure 3: if μ is chosen too small, then the propagated coherent structures will be diffused.

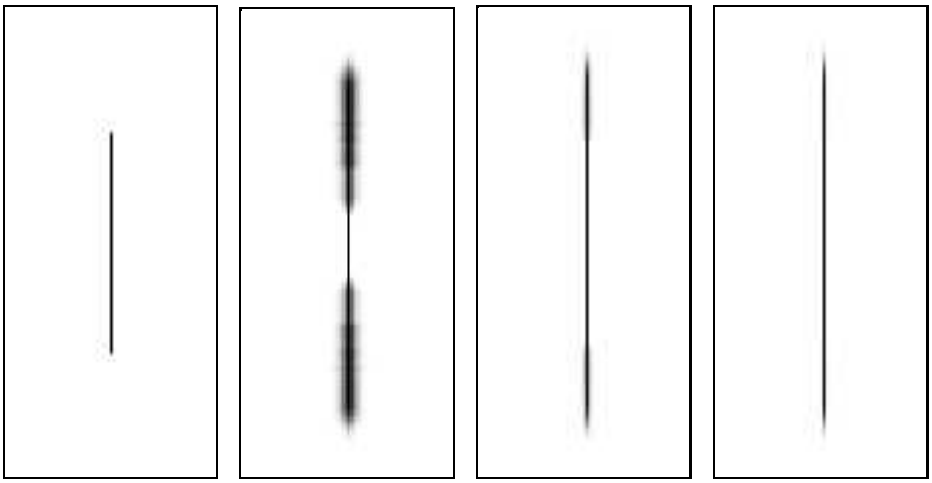

Fig. 3. From left to right: (i) Initial image, 106×238 pixels, (ii) eroded image after 50 time steps with $\Delta t = 0.5$, $\mu = 1$, (iii) analogously, but with $\mu = 2$, (iv) analogously, with $\mu = 4$.

We then define

$$\kappa \equiv \kappa\left(x, y, t\right) := \eta\left(v_2, \nabla u_\sigma\right)^\mu , \tag{10}$$

compare the discussion of (5)-(7). Because of $|\cos\left(\cdot\right)| \leq 1$ it is guaranteed that $\|\mathbf{D}\| \leq 1$. Note, that $\|\mathbf{D}\| = 1$ holds if and only if v_2 and ∇u_σ have identical orientations (which is not likely in a numerical computation).

3 The numerical method

The PDEs (2) are of *hyperbolic type* [7]. This means, in analogy to the Huygens principle of wave propagation, object boundaries are moved with or against the direction of their normal vector, depending on the given grey values. Thus, numerically, the task is to accurately approximate *moving fronts* given by the dilated/eroded object boundaries. A standard method for this purpose which we use here in a slight variation is the *Rouy-Tourin (RT) scheme*, see [14]. With the usual abbreviation $U_{ij}^n \approx u(i, j, n\Delta t)$, the method reads:

$$U_{i,j}^{n+1} \;=\; U_{i,j}^n \;+\; \kappa_{i,j}^n \Delta t \Big(\big[\max\big(0,\, U_{i+1,j}^n - U_{i,j}^n,\, U_{i-1,j}^n - U_{i,j}^n\big)\big]^2 + \big[\max\big(0,\, U_{i,j+1}^n - U_{i,j}^n,\, U_{i,j-1}^n - U_{i,j}^n\big)\big]^2 \Big)^{1/2}. \quad (11)$$

Specifying $\kappa_{i,j}^n = 1$ for all i, j, n, we retreive the original RT method. For more information on numerical methods for hyperbolic equations and more details concerning (11), we refer the interested reader to [3, 11, 12, 14].

4 Numerical experiments

We show two more experiments illuminating the capability of our method to enhance coherent image structures, supplementing the previous simple tests.

For the computation of κ, we use the procedure described in Paragraph 2, see especially (10). The parameters we use within the numerical experiments are set as $\sigma = 0.5$, $\rho = 4$, $\mu = 4$ and $\Delta t = 0.5$. For the computation of gradients, we use central differences for computing $\mathcal{S}$ and the Sobel operator for all other local gradients, respectively. These choices yield an accurate and efficient method.

We consider first an *synthetic image* featuring linear and round structures of several, randomly chosen orientation, and its anisotropic dilation, see Figure 3 (top row). We especially observe that interrupted lines are closed.

This desired outcome is also observable in real-world images, see Figure 3 (bottom row). The displayed image of a fingerprint is used as the initial condition for an anisotropic erosion process. Note, that our morphological anisotropic process does not introduce additional smoothing into the processed image.

5 Concluding remarks

We have shown that our method yields morphology-based anisotropic enhancement of images. In our ongoing research, we study extensions of the method for image areas where structures cross, which is a hard problem for algorithms for coherence enhancement. Furthermore, we investigate possibilities to make the scheme more accurate with respect to the estimation of local flow directions, so that even very large gaps in thin image structures (i.e., width of, effectively, one pixel) oblique to the grid orientation can be closed without directional deviation.

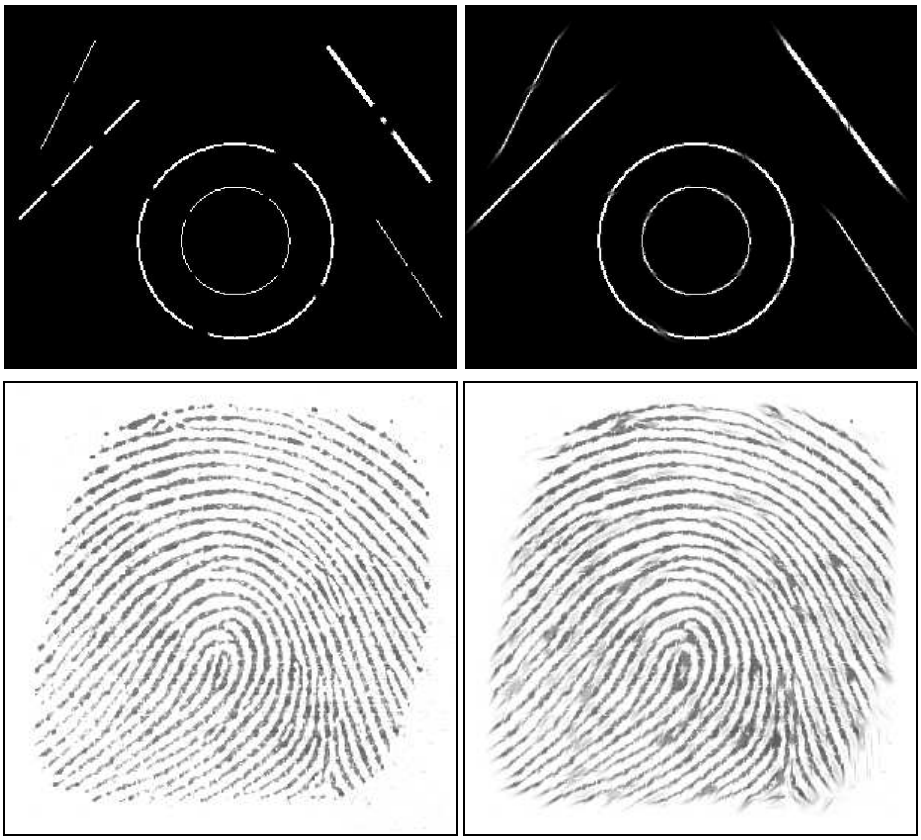

Fig. 4. (a) Top left: Synthetic image, 393 × 278 pixels. **(b) Top right:** Anisotropic dilation after 50 time steps. **(c) Bottom left:** Original image of a fingerprint with interrupted coherent structures, 300 × 300 pixels. **(d) Bottom right:** Anisotropic erosion of fingerprint after 20 time steps.

References

1. Alvarez, L., Guichard, F., Lions, P.-L., Morel, J.-M.: Axioms and fundamental equations in image processing. Archive for Rational Mechanics and Analysis **123** (1993) 199–257
2. Arehart, A. B., Vincent, L., Kimia, B. B.: Mathematical morphology: The Hamilton–Jacobi connection. In: Proc. Fourth International Conference on Computer Vision. IEEE Computer Society Press, Berlin, May 1993, 215–219
3. Breuß, M., Weickert, J.: A Shock-Capturing Algorithm for the Differential Equations of Dilation and Erosion. Journal of Mathematical Imaging and Vision **25** (2006) 187–201
4. Bigün, J., Granlund, G.H., Wiklund, J.: Multidimensional orientation estimation with applications to texture analysis and optical flow. IEEE Transactions on Pattern Analysis and Machine Intelligence **13** No. 8 (1991) 775–790

5. Brockett, R. W., Maragos, P.: Evolution Equations for Continuous-Scale Morphological Filtering. IEEE Transactions on Signal Processing **42** No. 12 (1994) 3377–3386
6. Dougherty, E. R.: Mathematical Morphology in Image Processing. Marcel Dekker, New York (1993)
7. Evans, L. C.: Partial Differential Equations. Graduate Studies in Mathematics **19**. American Mathematical Society, Providence (1998)
8. Förstner, W., Gülch, E.: A fast operator for detection and precise location of distinct points, corners and centres of circular features. In: Proc. ISPRS Intercommission Conf. on Fast Processing of Photogrammetric Data (Interlaken, June 2-4, 1987) (1987), 281–305
9. Heijmans, H. J. A. M.: Morphological Image Operators. Academic Press, Boston (1994)
10. Lerallut, R., Decencière, E., Meyer, F.: Image processing using morphological amoebas. In: Proc. 5th Int. Symp. on Mathematical Morphology. Kluwer (2005)
11. LeVeque, R. J.: Finite Volume Methods for Hyperbolic Problems. Cambridge University Press, Cambridge, UK (2002)
12. Osher, S., Sethian, J. A.: Fronts propagating with curvature-dependent speed: Algorithms based on Hamilton–Jacobi formulations. Journal of Computational Physics **79** (1988) 12–49
13. Perona, P., Malik, J.: Scale space and edge detection using anisotropic diffusion. IEEE Transactions on Pattern Analysis and Machine Intelligence **12** (1990) 629–639
14. Rouy, E., Tourin, A.: A viscosity solutions approach to shape-from-shading. SIAM Journal on Numerical Analysis **29** (1992) 867–884
15. Rao, A.R., Schunck, B.G.: Computing oriented texture fields. CVGIP: Graphical Models and Image Processing **53** (1991) 157–185
16. Sapiro, G., Kimmel, R., Shaked, D., Kimia, B. B., Bruckstein, A. M.: Implementing continuous-scale morphology via curve evolution. Pattern Recognition **26** (1993) 1363–1372
17. Serra, J.: Image Analysis and Mathematical Morphology, volume 1. Academic Press, London (1982)
18. Serra, J.: Image Analysis and Mathematical Morphology, volume 2. Academic Press, London (1988)
19. Soille, P.: Morphological Image Analysis. Springer, Berlin, second edition (2003)
20. van den Boomgaard, R.: Mathematical Morphology: Extensions Towards Computer Vision. PhD thesis, University of Amsterdam, The Netherlands (1992)
21. Weickert, J.: Anisotropic Diffusion in Image Processing. Teubner, Stuttgart (1998)
22. Weickert, J.: Coherence-enhancing diffusion filtering. Int. J. Comput. Vision **31** (1999) 111–127
23. Weickert, J.: Coherence-enhancing shock filters. In: B. Michaelis and G. Krell (eds.), Pattern Recognition. Lecture Notes in Computer Science, Vol. 2781. Springer, Berlin (2003) 1–8